

Direct phase-change cooling of vapour chamber integrated with IGBT power electronic module for automotive application

Yiyi Chen, Bo Li, Xuehui Wang, Xin Wang, Yuying Yan, Xiang Li, *Senior Member, IEEE*, Yangang Wang, *Senior Member, IEEE*, Fang Qi, Helong Li

Abstract— In electric vehicles and hybrid electric vehicles, IGBT power module trends to dissipate higher heat flux due to increased power rating and reduced package size. An inefficient cooling method will result in stringent thermal reliability problems. Therefore, there is a strong need for innovative and efficient cooling technologies in order to tackle these issues. In this paper, a localised direct phase change cooling strategy is applied and integrated with Direct Bonded Copper in IGBT power module. Vapour chamber with light weight, high thermal conductivity and even temperature uniformity replaces original copper baseplate. Layers of thermal grease and original cooling plate are removed, leading to a further reduction in thermal resistance. In order to evaluate the new module, a thermal model and an experiment were built to analyse temperature distribution in layers, junction temperature, temperature uniformity and thermal resistance. Results indicate the integrated thermal management system outperforms traditional cooling solutions on the cooling capacity. Improvements on junction temperature, temperature uniformity and total thermal resistance are 34.6%, 76.6%, and 41.6%, respectively. The results illustrate the potential of phase change cooling by vapour chamber. It provides a new perspective in the compact and efficient design of power electric modules.

Index Terms—IGBT semiconductor module, electric vehicles, phase change cooling, vapour chamber, thermal resistance

I. INTRODUCTION

Nowadays, popularisation of hybrid electric vehicles and electric vehicles becomes an overwhelming trend due to significant exhaust emissions reduction. Insulated gate bipolar transistor (IGBT) power module as a power switching transistor device is one of the most important components in power supply and motor control circuits. The heat flux of IGBT power module will continuously increase due to packaging system miniaturisation and power rating surge. Based on previous studies [1-3], in next

generation of hybrid electric vehicles, junction to coolant thermal resistance normalized to die area will decrease from 0.85 Kcm²/W to 0.17 Kcm²/W. Without proper thermal management technologies, excessively high temperature and uneven temperature can cause severe module failures such as solder-ceramic delamination and crack as well as bonding wire lift off. Therefore, it is required to develop highly efficient and compact cooling solutions for higher heat flux in IGBT modules.

A. State-of-art thermal management system

Single-phase cooling technologies included air, water-glycol, etc. are most-used in thermal management of IGBT modules. With increasing heat dissipation, however, it is predicted that conventional air cooling solution is difficult to meet cooling demand sufficiently, especially when the power dissipation exceeds up to 1500 W [4]. Micro-and mini-channel liquid cooling solutions were focused over the past decade. It has a major advantage of simplicity of heat sink design due to compact and light in weight. It can also offer a higher cooling capacity typically 120 W/cm² in comparison with that of air cooling (typically 50 W/cm²) [5]. Yin et al. [6] designed a rectangular micro-channel heat sink fabricated directly in the AlN-layer of substrate. The simulation results show the thermal resistance of the proposed structure is 0.128 K/W at a pressure drop of 66.6 kPa, which was reduced by 80% compared with conventional structure. Stevanovic et al. [7] developed an integral micro-channel heat sink for power electronics. An array of sub-millimetre channels was directly fabricated on back side of the substrate. The junction to fluid thermal resistance for IGBTs was 0.17 °C cm²/W. Brunschwiler et al. [8] investigated heat dissipation and pressure drop for arrays including in-line and staggered pins configurations and microchannel with an emphasis on interlayer cooling in 3-D IC stacks. Vafai et al. [9] proposed a numerical model to analyse two-layered micro-channel heat sink with respect to thermal performance and pressure drop. It was found that the streamwise temperature rise on the base surface and pressure drop were both reduced by comparison with one-layered heat sink. Naqiuddin et al. [10] reviewed micro-channel design for high heat flux application such as solar cell, fuel cell, heat exchanger and medical system. However, low temperature uniformity caused by flow redistribution, channel clogging erosion

(Corresponding author: Bo Li (first) and Xiang Li (second))

Yiyi Chen, Bo Li, Xuehui Wang, Xin Wang and Yuying Yan are with Faculty of Engineering, University of Nottingham, NG7 2RD Nottingham, UK (e-mail: yiyi.chen@dynexsemi.com; bo.li@nottingham.ac.uk; xuehui.wang@nottingham.ac.uk;

xin.wang1@nottingham.ac.uk; yuying.yan@nottingham.ac.uk)

Xiang Li and Yangang Wang are with Dynex Semiconductor Limited, Doddington Road, Lincoln, LN6 3LF, UK. (e-mail:

xiang.li@dynexsemi.com; yangang.wang@dynexsemi.com)

Fang Qi is with Coresing Semiconductor Technology Co., Ltd, Hunan, China. (e-mail: qifang@cszic.com)

Helong Li is with CREE Europe GmbH, Einsteinstrasse 12, 85716, Unterschleisheim, Germany. (e-mail: helong.li@cree.com)

and low term reliability is still needed to be carefully considered. In particular, heat transfer coefficient of micro channels strongly depends on the size of channel and fluid flow rate. Whereas, pumping power inevitably increases with heat transfer rate. In order to decrease the working load of pump, jet impingement becomes an attractive cooling method. It is able to generate high flow rate of fluid with lower pump and yield high local heat transfer rate. Agbim et al. [11] investigated the direct integration of single jet impingement for power electronics cooling. The experiments, analytical models and computation models were used to evaluate the influence of number of jet, jet to jet spacing and jet diameter on cooling performance. A reduction of up to 25% in total package thermal resistance was achieved. Liu et al.[12] established an unsteady numerical model to explore the impingement cooling performance of synthetic jets for electronic devices. This study investigated the effect of nozzle-to surface distance on thermal performance. It was found that the cooling capacity increases and then decreases with an increasing nozzle to surface distance. Besides, the significant recirculation phenomenon of hot air was found at small nozzle to surface distance, which deteriorated heat transfer. Nonetheless, temperature distribution of the cooled surface is non-uniform because cooling performance rapidly degrades when it is away from the center of the jet region. In order to improve temperature uniformity, array impingement cooling was paid more attention. To overcome this drawback, Yu et al.[13] designed various novel fluid diodes to form hybrid synthetic jets. It was found that the hybrid synthetic jet with a convergence nozzle generates the best cooling ability among various configurations. Natarajan et al. [14] designed and manufactured a complex ceramic cooling device with 1600 micron-size jets and 1681 interstitial returns. The device is able to dissipate more than heat flux of $2.5\text{MW}/\text{m}^2$ with a water pressure drop $<70\text{ kPa}$. Bhunia [15] carried out an experiment about an array impingement cooling system employing 441 nozzles, and each with diameter of $200\ \mu\text{m}$. Results indicated that the average heat transfer coefficient doesn't largely reduce and it is capable of cooling a few cm^2 area to a few hundred cm^2 area. Gould et al. [16] contrasted thermal performance of cold plat cooling, microchannel cooling and the array jet impingement cooling of silicon carbide power conversion module for vehicle application. The jet impingement cooling reduces junction to coolant thermal resistance by 2.8 and 1.7 times compared to cooling plate and microchannel cooler. Wei et al.[17-19] conducted several researches on direct single and multi-jet impingement cooling to improve temperature uniformity and reduce the cost. They fabricated 3D printed jet impingement coolers applied to 2.5D Si interposer packages. 3D printing has attracted a lot of attention to fabricate cost efficient polymer impingement coolers. It is of benefit to reducing the material cost and print complex structure in one piece[17]. However, current 3D printing technology still has several limitations to produce polymer based structure with sub-mm size. In general, heat flux levels of around $250\ \text{W}/\text{cm}^2$ and $1,000\ \text{W}/\text{cm}^2$ for water have been reported for single-phase and phase change impingement, respectively [20-23]. Although jet impingement can achieve a very high heat transfer

coefficient, the applicability of this strategy is limited by problems of complex cooling flow redistribution, cooling loop leakage and channel blockage.

B. Integration of direct bonded copper substrate to vapour chamber

Vapour chamber, as a phase change cooling component, is a super heat conductive device and it now represents an appealing option for efficient cooling electric components. Vapour chamber is a vacuum metallic container with wick structure lining the internal walls saturated with working fluid. It utilizes cyclic phase change heat transfer process which can absorb much more heat than single-phase heat transfer process. Generally, a vapour chamber effective thermal conductivity is in range of $1,000\ \text{W}/\text{cm}^2$ to $50,000\ \text{W}/\text{cm}^2$ [6]. Fig. 1 illustrates the operational principle of a vapour chamber. In this case, as heat dissipated by IGBT chips and diodes is applied, the working fluid will immediately vaporise to fill the vacuum. Then vapour releases its latent heat of vaporisation and condenses when it comes into contact with a cooler wall surface. After that, condensed fluid returns to the heat sources due to capillary action in sintered copper wick structure lined inside wall, ready to be vaporized again and repeat the cycle. The capillary force of wick structure enables vapour chamber to overcome gravity and work in any orientation. Recently, interest has grown in extending the use of vapour chambers to high heat flux electronics cooling due to its high temperature uniformity, fast heat removal capacity, compactness, flexible design and high integration. However, vapour chamber needs to be carefully designed to avoid dry out and high initial cost is also an issue of vapour chamber.

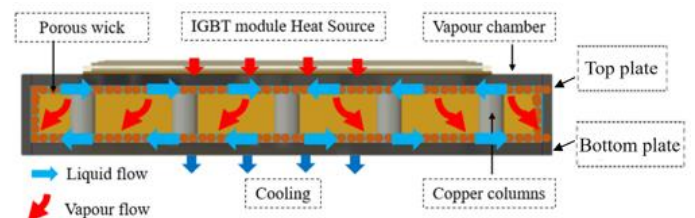


Fig. 1. Schematic of working principal of vapour chamber with bonded IGBT substrate (image for illustration)

Table I lists parameters of vapour chamber heat sink in this study. The size of vapour chamber is compact and the same as the area of IGBT module. The most common envelope/wick and working fluid combinations are copper/water for electronics cooling. Filling weight of 4.1g is used for this study. The wick structure is made up of copper foam with porosity of 69.8%. The copper foam is oriented within the whole chamber pressed against the top and bottom copper plates. 36 copper solid columns with diameter of 3 mm throughout the vapour chamber to support the plates. The top and bottom plates are sealed around the perimeter via diffusion bonding. Figure 2 displays the interior structure and wick structure.

Compared with copper baseplate, vapour chamber has much higher thermal conductivity, more uniform temperature distribution, more durable and lightweight. Moreover, vapour chamber can be integrated into many heat sinks such as pin fin structure. Li et al. and Wang et

al.[24-29] conducted many researches on vapour chamber and heat pipe with respects of wick structure and ultra-thin flattened heat pipes. Avenas et al. [30], Chen et al.[31], Qi et al. [32] and Hose [33] developed a power module with vapour chamber heat spread. Wang et al.[34] experimentally investigated EV battery cooling and heating by using heat pipes. Chen et al. [35] designed and fabricated a novel ultra-thin vapour chamber with a thickness of 0.4 mm. Compared with the electronic module



(a) Interior structure of vapour chamber without wick structure (Bottom plate)



(b) Copper foam wick of vapour chamber

Fig. 2 Interior structure of vapour chamber

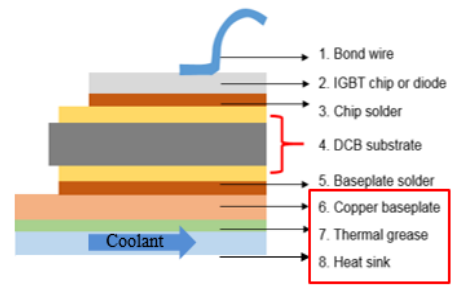
without ultra-thin vapour chamber, 54% and 8% were reduced in the maximum surface temperature difference and heating block temperature. Ivanova et al. [36] proposed heat pipe directly integrated into DBC (Direct bonded copper) for cooling of power semiconductor module packaging. As a result, it can reduce the high heat flux to a lower and manageable level which can be dissipated through traditional cooling solution. Bose et al. [37] experimentally and numerically investigated the thermal performance of a vapour chamber for electronic cooling applications. The maximum temperature reduces by 26% and the mean deviation in temperature distribution is decreased from 12.5% to 9% compared with processor without vapour chamber. Shwin-Chung Wong et al. [38] made a vapour chamber with parallel groove and found that it has good thermal performance with low thermal resistance and large thermal limit under different orientations.

TABLE I
VAPOUR CHAMBER PARAMETERS

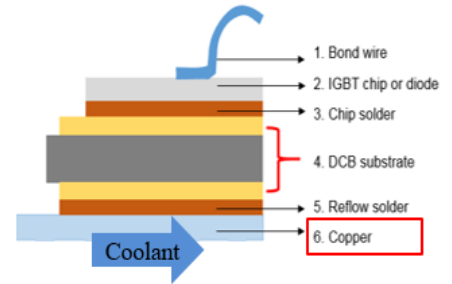
Parameter	Value
Vapour chamber size	122 mm(L)×62mm (W)×3 mm(H)
Vapour chamber casing material	Copper
Vapour chamber working fluid	Water
Vapour chamber filling weight	4.1g
Type of wick structure	Sintered copper
Porosity of wick structure	0.698

As illustrated in Fig. 3, it includes cross sections of three different IGBT semiconductor power modules with

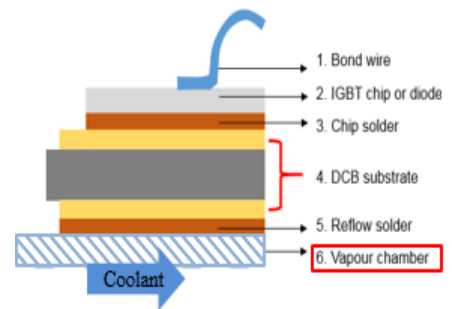
thermal management structures. Fig. 2(a) represents conventional indirect cooling. IGBT module with copper baseplate is bolt to heat sink by using thermal grease-based thermal interface material (TIM). TIM layer is one of the largest contributions to total thermal resistance which is the major impact on improving cooling capacity.



(a)



(b)



(c)

Fig. 3. Structure of IGBT (a) Case A traditional indirect cooling (b) Case B direct cooling attached with copper baseplate IGBT module (c) Case C with direct cooling attached with vapour chamber baseplate

Based on the prototype used in this study, a comparison of steady state relative thermal resistance of each part and overall IGBT power modules is shown in Fig. 4. It is obvious that the direct cooling structures don't have thermal grease and additional heat sink. The thermal resistance of Fig. 3(b) shows a cross section of an assembly using direct attach method. DBC layer is directly soldered on a copper baseplate. Currently, this direct cooling of power semiconductor module is most commonly adopted due to its compact structure. In this structure, thermal grease and additional aluminium heat sink are removed and they account for 25.8 % of overall thermal resistance of case A. For further improvements on thermal resistance reduction, in our new design, copper baseplate is replaced by vapour chamber which is integrated into substrate as shown in Fig. 3(c). The overall thermal resistance is reduced by 32.2% by comparing to the structure of case A.

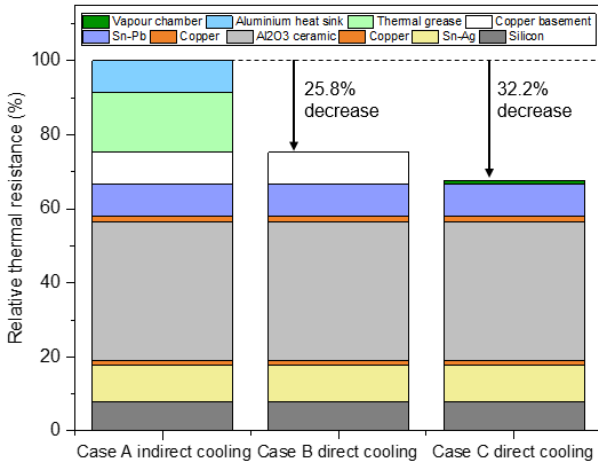


Fig.4. Comparison of thermal resistance between convensional structures and novel structure

C. Thermal failure mechanisms in IGBT power modules

The main cause of thermal failure is repetitive thermomechanical stress due to power and thermal cycling. Generally, higher temperature, various temperature gradient in system components consisting of different material, large coefficient of thermal expansion mismatch and mismatch in length of adjacent layer result in thermal stress and forces at the interface between adjoining materials. IGBT power module is exposed to thermal stress when the IGBT power module starts to operate, which continually affects adjacent layers, solder layers and wire bonding. Consequently, IGBT may suffer from some main failure modes.

Bonding wire with a diameter of 100-500 μm usually suffers lift-off and heel crack mechanism, which is mainly attributed to crack propagation induced by coefficient of thermal expansion between aluminium and silicon and power cycling [1]. The origin of thermal fatigue of substrate is the coefficients of thermal expansion difference between copper and ceramic. It is also observed that thermal fatigue life of the substrate is depended on the growth of a fatigue crack from a geometric singularity and close to the interface between upper copper and ceramic layer [2]. Another dominant failure mechanism is solder joint fatigue. Solder joints are used for joining chip and substrate, and substrate and baseplate in IGBT. They have a lower melting temperature, yield stress and higher coefficient of thermal expansion compared with other packaging layers, thus the deformation of solder is highly dependent on the temperature and strain rate [39]. With an increase in temperature and thermal stress, creep, voids, delamination and crack of the solder will be accelerated, leading to thermal resistance increase and junction temperature growth, and then accelerating module failed. Therefore, it is important to accurately predict thermal performance in the design and reliability of electrical power devices [40]. These mentioned failure modes will finally lead to IGBT power module burnout or latch up.

In this paper, a new IGBT power module with phase-change direct cooling is developed. This cooling strategy mainly focused on mitigating the effect of hot spots, reducing thermal resistance, increasing temperature uniformity, and improving the lifetime. In our design, the

origin copper baseplate is replaced with a vapour chamber with a phase change inside of chamber original and the chamber is directly soldered onto the DBC layer. Chilled water directly cools the bottom side of the vapour chamber and removes heat away. This cooling strategy with compact structure and highly efficient heat transfer provides the opportunity of an individual cooling method of power electronic modules, such as MOSFETs or IGBTs.

II. STUDY METHODOLOGY

Based on the structure of the case 3b and case 3c, a thermal model is established by using finite element method to investigate thermal performance under power cycle. Also, an experiment is built to compare the thermal performance of the vapour chamber direct cooling and conventional copper direct cooling of IGBT power modules at various operating power loss conditions.

A. Simulation model

The simulation is conducted by Comsol Multiphysics software. It is found that the simulation results of temperature distribution remain almost unchanged after the density exceeds 222,646. Therefore, mesh with an element count of 222,646 is selected for this study. Figure 5 shows the detail of final mesh of the module. The size of mesh ranged between 2 mm and 0.5 mm. Thin and weak components such as solder layers, chips and DBC are finely meshed whereas the baseplate are coarsely meshed.

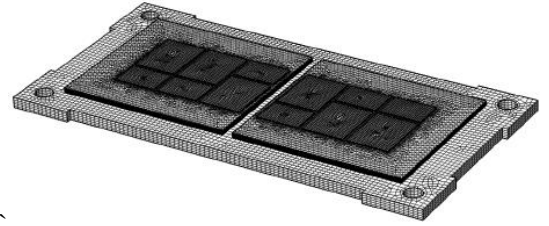


Fig.5 Finite element mesh of the module

The simulation method is used to simulate for heat transfer of IGBT power module. The thermal modelling includes the real power loss. With this strategy, it is able to identify the potential hot spots, maximum junction temperature and temperature gradient on IGBT power module. The thermal simulation is validated against experiment results. In thermal modelling, the diffusion-convection governing energy equation is used to solve temperature field problem as expressed in equation 1. This equation neglects mass transport part.

$$\rho C_p \frac{\partial T}{\partial t} - \nabla(k \nabla T) = Q + q_s T \quad (1)$$

where ρ , C_p , k , Q and q_s are the density, heat capacity, thermal conductivity, heat generation and absorption/production coefficient respectively.

In thermal boundary setup, parameters of each model are given in Table II. The convective heat transfer coefficient of water heat sink which provides cooling to the bottom of baseplate are assumed as 800 $\text{W/m}^2\text{K}$ and 1200 $\text{W/m}^2\text{K}$ corresponds to copper baseplate case and VC baseplate case based on experimental data.

TABLE II
BOUNDARY CONDITION IN IGBT MODELLING

Boundary condition	Value
Initial module temperature	20°C
Heat source from pre FRD	19W
Heat source from pre IGBT	61W
Coolant temperature	20°C
Heat transfer coefficient of air	30W/m ² K

In a semiconductor device such as an IGBT or a diode, there are three categories of power losses as shown in (2) – (6). The first category is the conduction loss which consists of the heat dissipation from IGBT PSS and diode PDC. The second category is switching losses PSW and includes the energy lost when the device is switching ON or OFF. The third category is named recovery loss of diodes Prec and regards the losses when the device is fully OFF.

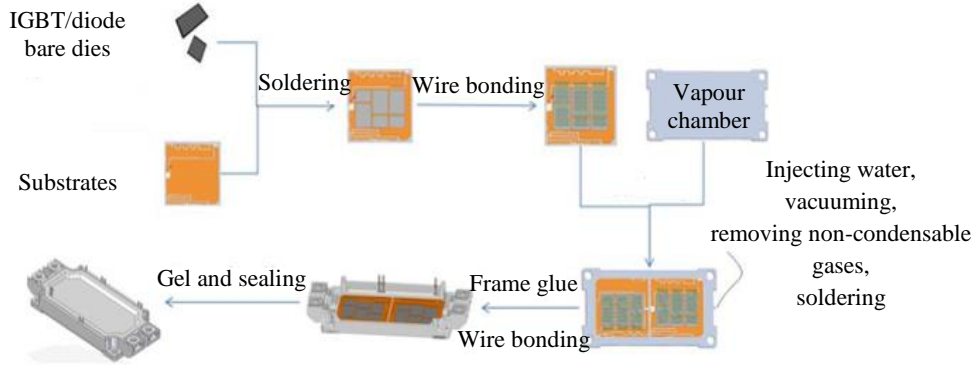


Fig.6 Fabrication process of IGBT semiconductor integrated with vapour chamber

$$P = P_{SS} + P_{SW} + P_{DC} + P_{rr} \quad (2)$$

where conduction losses from IGBT PSS and diode P_{DC} are defined, respectively, as

$$P_{SS} = I_{CP} \times V_{CE(SAT)} \times \left(\frac{1}{8} + \frac{D}{3\pi} \cos\phi \right) \quad (3)$$

and

$$P_{DC} = I_{CP} \times V_f \times \left(\frac{1}{8} - \frac{D}{3\pi} \cos\phi \right) \quad (4)$$

where I_{CP} , $V_{CE(SAT)}$, D , $\cos\phi$, V_f are peak value of output current, forward voltage drop in IGBT, duty ratio, power factor, forward voltage drop in the diode.

Switching losses PSW of each IGBT typically contribute a large amount to the total system losses. It can be described as

$$P_{SW} = (E_{SW(ON)} + E_{SW(OFF)}) \times \frac{f_s}{\pi} \quad (5)$$

where $E_{SW(ON)}$, $E_{SW(OFF)}$ is the switching on loss of IGBT and switching off loss of IGBT. f_s is the switching frequency.

During switching from the conduction to block state, a diode stored charge which must be discharged. The power loss from this stage is called recovery loss of diodes Prec given by (6).

$$P_{rec} = E_{rec} \times \frac{f_s}{\pi} \quad (6)$$

where E_{rec} is the recovery loss of diode.

In this study, we focus on the operation condition at frequency of 6200 Hz. Therefore, based on the calculation, power loss applied to each IGBT chip and diode are 61 W (high state) and 19 W (low state). Top switch and bottom switch operate alternatively. At top switch power loss stage, three top switch IGBTs and diodes firstly start to work and dissipate 183 W heat in total during 0 μ s -56 μ s, and then top diode generates totally 57 W during 56 μ s-80 μ s. And then, bottom switch IGBT and diode operate in the same way. Top switch and bottom switch operate alternatively.

B. Experiment

1) Integration process of a IGBT with vapour chamber

Fig. 5 shows the integration processes of IGBT power module with vapour chamber. After finishing the IGBT/diodes soldering on substrate and wiring bonding process, the substrate is soldered onto the vapour chamber

baseplate by using reflow soldering. At this stage, working fluid is not injected into vapour chamber since high temperature can lead to vaporization of working fluid and large deformation of vapour chamber during soldering process. After soldering process, water is injected through a tube and the chamber is vacuumed. Next, non-condensable gases are moving into the tube by heating the vapour chamber. And then the tube is removed and sealed. Fig. 6 shows the prototype of IGBT integrated with vapour chamber.

2) Experiment setup

After going through all fabrication processes described in Fig. 6, the final prototype of IGBT integrated with vapour chamber has been completed, as shown in Fig. 7. It is used to experimentally investigate thermal behaviour with respects of junction temperature, thermal resistance and heat transfer coefficient of IGBT semiconductor module. Junction temperature is the crucial factor monitoring reliability of power modules and thermal resistance is a good indicator to quantify the cooling capacity of cooling devices. Fig.8 displays entire schematic diagram of experiment apparatus and structure of IGBT semiconductor module with vapour chamber thermal

management

system.

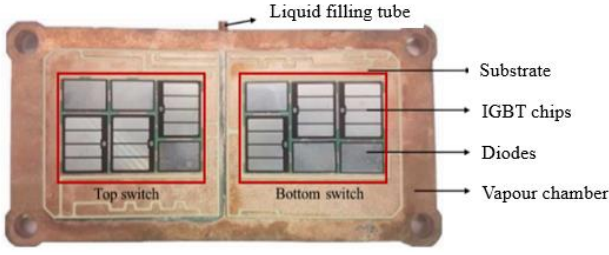


Fig. 7. Schematic of the analysed power module prototype

The vapour chamber is directly soldered on DBC substrate by using Sn-Pb solder material and it is bolted with a water-cooled plate. Constant heat load is directly transferred to each diode and IGBT chip by six cartridge heaters through the copper heating blocks. The effective heating areas are the same as that of IGBT chips and diode. The IGBT chips and diodes are directly attached to the copper heating block, and the whole module is sandwiched between heating block and copper water cooling plate by screw installations. A range of 30 W to 240 W heat power is fed into 6 cartridge heaters equally by incremental of 30 W. A chiller continuously generated cold water with a temperature of 20 °C and water flow rate is set to 40 L/h. Thermal grease, TIG780-38 (thermal conductivity 3.8 W/mK) is used between the heater and the IGBT chips and diodes to minimise the thermal contact loss. There is no thermal grease introduced between bottom surface of vapour chamber and water cooling plate since chilled water is directly contacted with bottom surface. Type T thermocouples are placed on water inlet, outlet, and IGBT semiconductor module as shown in Fig. 9. A mineral wool insulation with thermal conductivity of 0.044 W/mK covers the whole test section and the test rig is placed in a PU enclosed container with thermal conductivity of 0.02 W/mK to prevent heat loss to the ambient.

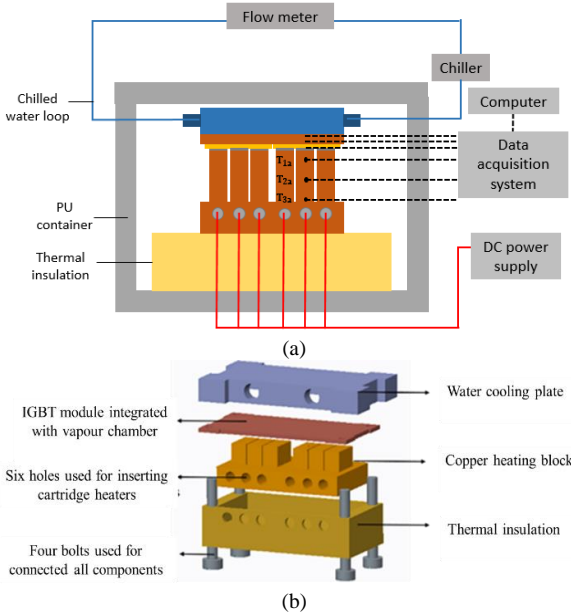


Fig. 8. (a) Schematic diagram of experiment apparatus (b) Schematic diagram of IGBT power model with heat sink and heat source

3) Data acquisition and uncertainty analysis

In this study, we managed to measure thermal resistance of vapour chamber and whole IGBT semiconductor module

with vapour chamber integrated module. Thermal resistance R_{VC} is derived by

$$R_{VC} = \frac{\bar{T}_t - \bar{T}_b}{Q} = \frac{\frac{1}{5} \sum_1^5 T_i - \frac{1}{4} \sum_7^{10} T_i}{Q} \quad (7)$$

Where \bar{T}_b and \bar{T}_t are the average temperature of bottom evaporator surface and condenser top surface of vapour chamber receptivity, and Q is the heat input through copper heater surface. Average temperatures are calculated by using arithmetic mean of the related probes when the system is at steady state.

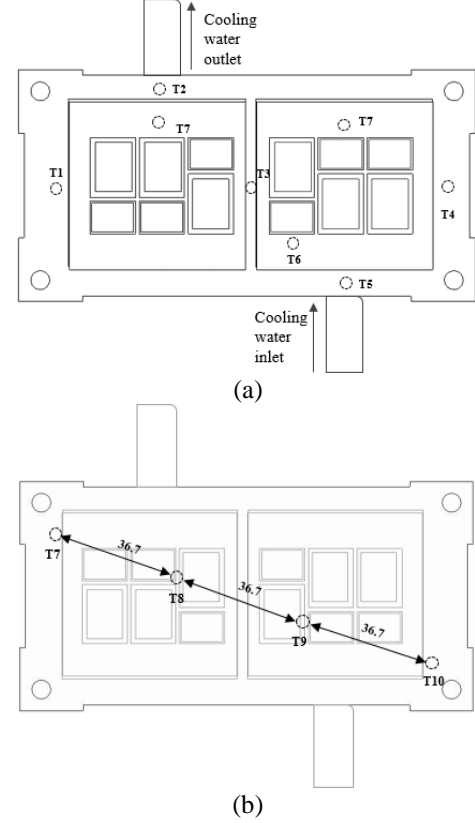


Fig. 9. Positions of the thermocouple on (a) bottom surface contacted with heat source and (b) top surface contacted with heat sink

Fig. 10 shows thermal resistances of IGBT semiconductor module with vapour chamber thermal management system in the heat path from junction to ambient. The total thermal resistance between chip and cooling media $R_{th(j-a)}$ is the total thermal resistance of IGBT with thermal management power module, which includes thermal resistance between chip and baseplate $R_{th(j-b)}$, and heat sink cooling media $R_{th(b-a)}$, as expressed as

$$R_{th(j-a)} = R_{th(j-b)} + R_{th(b-a)} \quad (8)$$

$$R_{th(j-b)} = \frac{\bar{T}_j - \bar{T}_b}{Q} = \frac{T_6 - \frac{1}{4} \sum_7^{10} T_i}{Q} \quad (9)$$

$$R_{th(b-a)} = \frac{\bar{T}_b - T_a}{Q} = \frac{\frac{1}{4} \sum_7^{10} T_i - T_a}{Q} \quad (10)$$

Where T_a and T_j represent cooling media temperature and junction temperature respectively. It is impractical to directly measure junction temperature T_j of the semiconductor module[41]. In this study, thermocouples

are placed as close as possible to IGBT chip to measure the junction temperature.

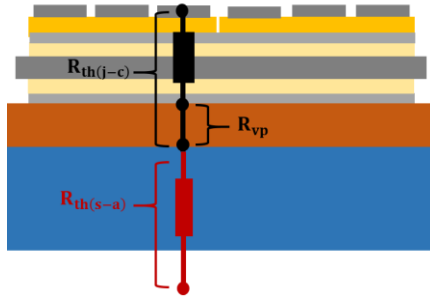


Fig. 10. Fractions of calculated thermal resistance in the IGBT semiconductor module integrated with vapour chamber

Table III lists the uncertainties of main parameters. An uncertainty analysis is used to determine the uncertainties involved in this experiment. The uncertainty analysis of total thermal resistance is given by (11). From the uncertainty analysis, it is observed the maximum uncertainty with total thermal resistance is less than 7%.

TABLE III
UNCERTAINTIES OF MAIN PARAMETERS

Parameter	Unit	Uncertainty
Temperature	°C	±0.4%
K_{CU}	W/mK	2.2%
Voltage	V	±0.8% of reading
Machining error-Distance	m	2%
Current	A	±1.2% of reading
Data logger		0.1%

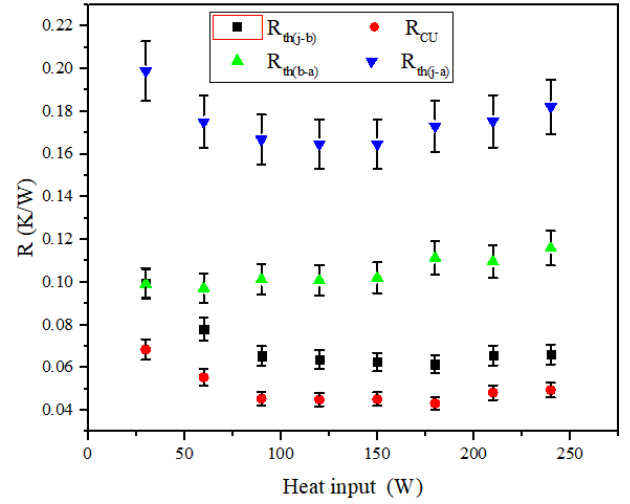
$$\frac{\Delta R_{j-a}}{R} = \sqrt{\left(\frac{\Delta Q}{Q}\right)^2 + \left(\frac{\Delta T_{j-a}}{T}\right)^2} \quad (11)$$

III. EXPERIMENT THERMAL PERFORMANCE RESULTS

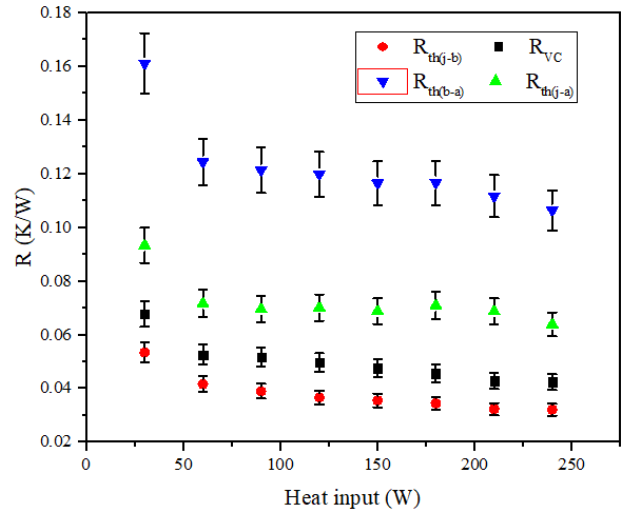
A. Thermal resistance verification and heat transfer coefficient of IGBT module

The thermal resistance of vapour chamber R_{VC} , thermal resistance between chip and baseplate $R_{th(j-c)}$, heat sink and cooling media $R_{th(c-a)}$ and the total thermal resistance between chip and cooling media $R_{th(j-a)}$ are plotted as a function of heat power input in Fig. 11. The thermal resistance of copper baseplate reduced from 0.068 K/W to 0.055 K/W with heat input power ranged between 30 W and 60 W and then it is kept between 0.045 K/W and 0.049 K/W with heat input increase from 90 W to 240 W. The thermal resistance of vapour chamber continuously decreases from 0.053 K/W to 0.032 K/W when heat input ranges between 30W and 240W, which is attributed to phase change heat transfer. At the low heat input, the water film in vapour chamber is thick and boiling is at incipient stage, which leads to high evaporation and condensation thermal resistance. With increase in heat input, water film recession and more water turns into vapour by absorbing heat from evaporator wall of vapour chamber and the boiling process is enhanced. Therefore, the water film becomes thinner and the evaporation and condensation thermal resistance reduces[42]. Regarding $R_{th(b-a)}$, it mostly

depends on the thermal performance of baseplate since the water flow rate, water temperature and other boundary conditions are kept the same between IGBT with vapour chamber and copper cases. Therefore, IGBT with vapour chamber baseplate has a lower thermal resistance of water cold plate than IGBT with copper baseplate and it is found that $R_{th(b-a)}$ is reduced with R_{VC} . In general, the total resistance $R_{th(j-a)}$, $R_{th(j-b)}$, and $R_{th(b-a)}$ also decrease with increase in heat input in vapour chamber module. Vapour chamber module can reduce 34.9%, 35.8%, 44.9% and 41.6% of thermal resistance of baseplate, $R_{th(j-b)}$, $R_{th(b-a)}$ and total thermal resistance $R_{th(j-a)}$ compared with copper module, respectively.



(a)



(b)

Fig. 11. Thermal resistance of IGBT power module under different heat loads (a) Copper baseplate (b) Vapour chamber baseplate

The verification of thermal resistance measurement is conducted by using Mentor Graphic test platform, as shown in Fig. 12. In this experiment, the junction to baseplate thermal resistance of IGBT with copper baseplate is measured to verify the thermal resistance. The junction to copper baseplate is as low as 0.062 K/W in Fig. 11 (a). In Fig. 12, chips of the IGBT with copper baseplate are heated by current and a cooling plate is used as heat sink to dissipate heat. A low testing current is applied to sense the

$V_{ce(on)}$, which is then transformed into junction temperature. This test platform measures the distribution of thermal capacitance along the heat flow path, where the position on this path is expressed by the cumulative thermal resistance. To obtain the junction to baseplate thermal resistance, three different thermal interface materials are applied between IGBT baseplate and the cooling plate to identify the splitting point in the thermal transient curves. As shown in the Fig.13, there are three measurements with different thermal contacts which are dry contact, graphite contact and thermal grease contact. These three curves separate at the point where the heat flow changes. Therefore, the separation point of three curves (0.059 K/W) indicates the junction to copper baseplate thermal resistance of IGBT module. EconoDual module fabricated by Infineon has the same size and structure as the module used in this experiment. Based on the technical information[43], the junction to baseplate thermal resistance is 0.06 K/W, which is close to the verified thermal resistance of 0.059 K/W and 0.062 K/W in Fig.10.

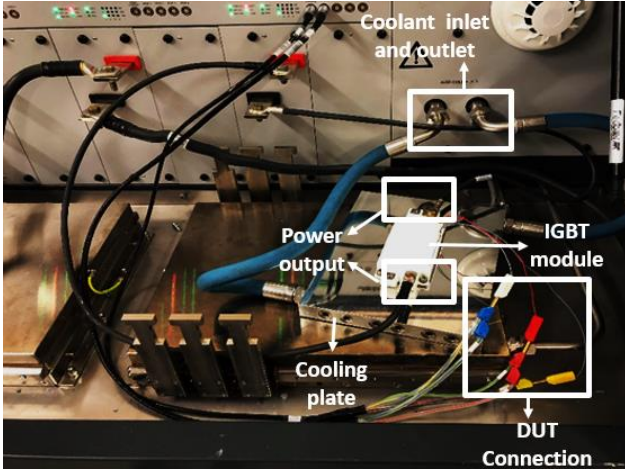


Fig. 12. Verification test facilities

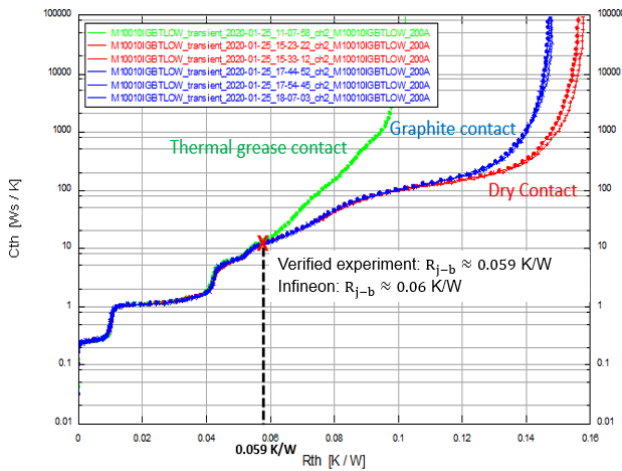


Fig. 13. Thermal resistance of IGBT module with different thermal interface materials

To evaluate the baseplate heat sink thermal performance, heat transfer coefficients of vapour chamber and copper baseplate heat sinks are calculated as shown in Fig.14. The results demonstrate that the phase change heat transfer coefficient for vapour chamber baseplate heat sink is much higher than single-phase heat transfer coefficient for copper baseplate heat sink, especially for high heat flux. Heat

transfer coefficient of vapour chamber heat sink increases with heat flux since more nucleation sites become active and bubble formation increases.

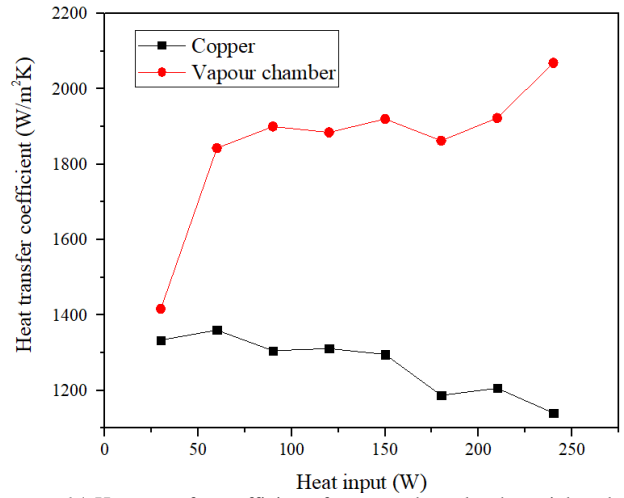
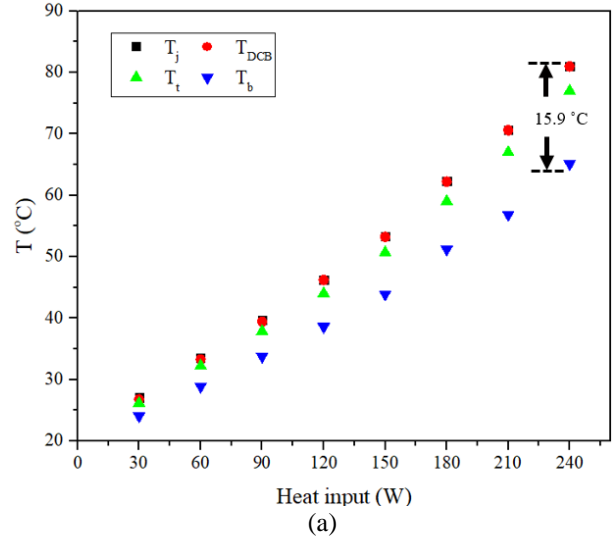


Fig. 14. Heat transfer coefficients for copper baseplate heat sink and vapour chamber baseplate heat sink

B. Temperature profiles in vapour chamber

Junction temperature is the crucial factor which affects the reliability of IGBT semiconductor significantly. Fig. 15 depicts temperature at junction, DBC layer, evaporation surface of vapour chamber/copper and condensation surface of vapour chamber/copper under different heat flux. In this experiment, the heat power input of copper and vapour chamber case varied from 30 W to 240 W in a step of 30 W respectively. It can be seen that DBC temperature T_{DBC} is close to junction temperature T_j for both cases, since thermal resistance of chip and chip solder layer have low thermal resistances. The temperature difference is closely related to thermal resistance. As heat input increased, the temperature difference between junction and vapour chamber condensation surface increases more slowly than the temperature difference between junction and cold surface of copper baseplate. The highest junction temperature of copper case is as high as 81.99 °C compared with 53.45 °C of vapour chamber case at the same applied power of 240 W.



(a)

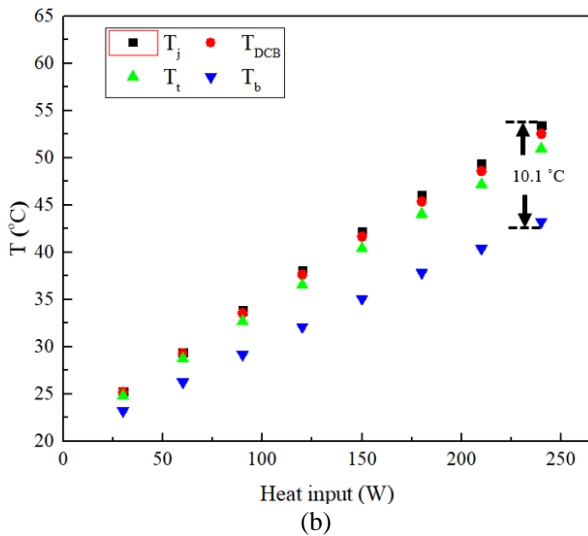
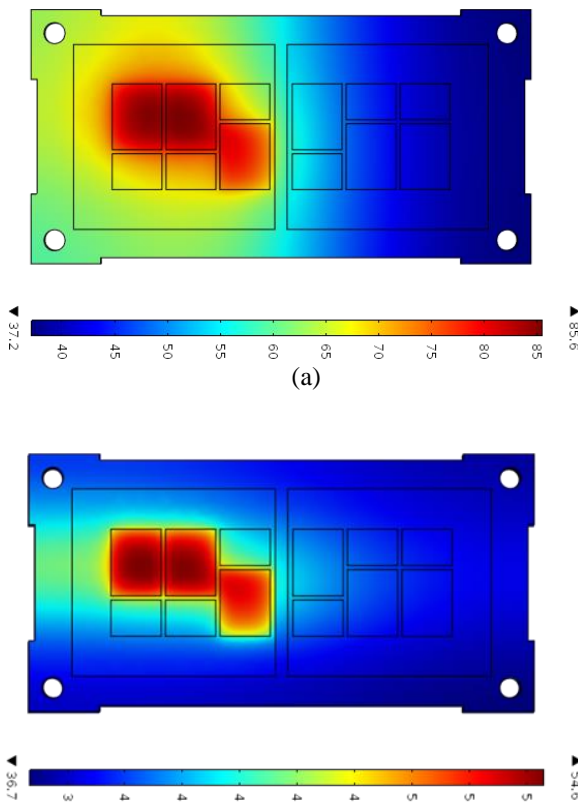


Fig. 15. Temperatures measured on IGBT module under different heat input power (a) Copper baseplate (b) Vapour chamber baseplate

To compare with simulation results, the junction temperature of copper and vapour chamber case obtained by finite element method are 85.6 °C and 54.6 °C respectively, as shown in fig.16. It can be found that the simulation model provides a good agreement with the experimental data in term of junction temperature. Furthermore, vapour chamber module has a smaller temperature difference between junction and condenser surface than copper baseplate module. These results demonstrate that vapour chamber is more effective at cooling than copper baseplate.

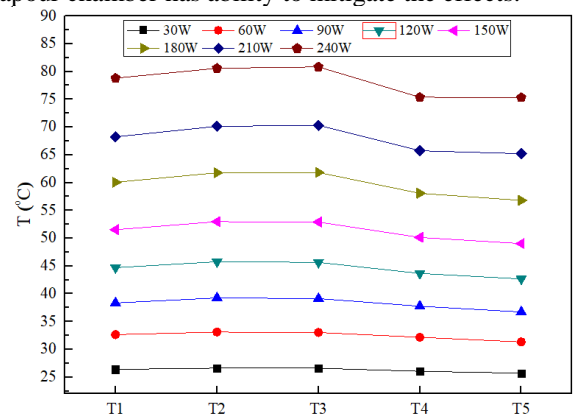


(a) Fig. 16. Temperature distribution (a) IGBT semiconductor with copper baseplate at stage of top switch igt power loss (b) IGBT semiconductor with vapour chamber baseplate during top switch IGBT at stage of top switch igt power loss

High-temperature uniformity is another important requirement for thermal management of power module. If a cooling device generates a low uniformity cooling performance, large temperature variation in packaging components with different properties and size cause forces at the interfaces between adjacent materials [17]. Thus, high-temperature non-uniformity within material layers also need to be responsible for the high stresses experienced by the packaging. This will jeopardize the reliable and efficient operation of the IGBT module. Therefore, thermal management system is required to achieve uniform cooling within a few degrees among whole IGBT components in the module.

Fig.17 and Fig.18 show the temperature distributions on the evaporator surface of the vapour chamber and copper baseplate under different heat inputs. With increase in power input, the temperature difference on the surface of copper baseplate increases quicker than that of vapour chamber. The maximum temperature difference of copper and vapour chamber baseplate are 5.52 °C and 1.29 °C at heat power input of 240 W, respectively. It is obvious that the IGBT with vapour chamber has a lower temperature and better temperature uniformity than IGBT with copper baseplate at the same heat load. The maximum temperature on the surfaces of vapour chamber and copper baseplates are both found at the position of T₃, being the center of the vapour chamber closest to the heat source.

The non-uniformity of temperature is mainly attributed to water cooling system and heater. Based on heat transfer mechanism, the temperature should be the same if the measured points locate same distance from heater. However, the experiment results show T₁ and T₂ are higher than T₄ and T₅ respectively for both vapour chamber and copper case, which can be explained that T₁ and T₂ are placed near the outlet of water and T₄ and T₅ located near inlet of water. The temperature of the area near the water inlet is definitely lower than that of the area close to water outlet, so more heat can be transfer to heat sink and the area near water inlet has a lower temperature. Nevertheless, vapour chamber has ability to mitigate the effects.



Thermocouple position on the evaporator surface of copper baseplate
Fig. 17. Temperature distributions on the copper baseplate under different heat load

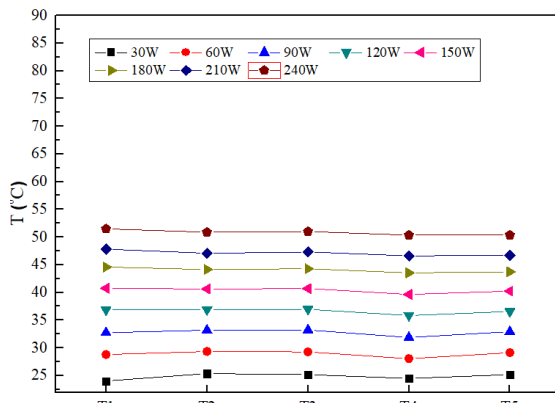


Fig. 18. Temperature distributions on the evaporator vapour chamber baseplate under different heat load

IV. CONCLUSION

Due to increase in power rating and miniaturization, IGBT power modules inevitably dissipate more heat flux density and thermal management becomes a major consideration. In this study, a new IGBT power module with phase change direct cooling is developed. This cooling strategy mainly focused on mitigating effect of hot spots, reducing thermal resistance and improve temperature uniformity. In this design, a vapour chamber replaces the typical copper baseplate and is directly soldered on the DBC. Chilled water directly contacts with bottom side of vapour chamber and removes heat away. Compared with indirect cooling solution, thermal grease layer with high thermal resistance and additional baseplate are removed, which leads to reducing of thermal resistance significantly. This novel cooling strategy with flexible shape, size and even material provides the opportunity of individual cooling method of power electronic modules, such as MOSFETs or IGBTs.

Experiments are conducted to investigate thermal performance of IGBT integrated with a vapour chamber and original copper baseplate. Furthermore, a computational heat transfer model is built to predict the junction temperature from the experimentally measured from heat transfer coefficient data. Based on the results, the new IGBT power module with vapour chamber provided a higher heat dissipation ability and better temperature uniformity compared with traditional IGBT power module with copper baseplate. At stationary heat load of 240 W, the junction temperature of IGBT with copper baseplate is up to 81.00 °C compared with 53.45 °C of vapour chamber case. High-temperature uniformity is also an important requirement for power module since large temperature difference will increase thermal stress and lead to many thermal reliability problems. The experimental results show temperature differences on the hotter surface of copper and vapour chamber baseplate are 5.52 °C and 1.29 °C, respectively. This indicates vapour chamber has better temperature uniformity than copper baseplate. Besides lower thermal resistance of vapour chamber could also increase the heat removal rates of cooling water. The results show vapour chamber module can reduce 34.9%, 35.8%, 44.9% and 41.6% of thermal resistance of baseplate, $R_{th(j-b)}$,

$R_{th(b-a)}$ and total thermal resistance $R_{th(j-a)}$ respectively compared with copper module.

ACKNOWLEDGEMENT

This project has been supported in the frame of the European Centre of Power Electronic Joint Research Programme (ECPE) and the Innovate UK - Advanced Propulsion Centre Programme 113167, and also supported by the Royal Society project 1130182 and European Union project H2020 - MSCA - RISE 778104.

NOMENCLATURE

CU	Copper	
DBC	Direct bonded copper	
EV	Electric vehicle	
IGBT	Insulated-gate bipolar transistor	
MOSFET	Metal oxide semiconductor field-effect transistor	
TIM	Thermal interface material	
VC	Vapour chamber	
A	Coolant covered surface area	m ²
C _p	Heat capacity	J/kg/K
h	Heat transfer coefficient	W/m ² K
k	Thermal conductivity	W/mK
Q	Heat input	W
R _{CU}	One dimensional thermal resistance of copper	K/W
R _{th(b-a)}	Thermal resistance of heat sink	K/W
R _{th(j-a)}	Total thermal resistance	K/W
R _{th(j-b)}	Thermal resistance between chip and baseplate	K/W
R _{VP}	Thermal resistance of vapour chamber	K/W
T _a	Cooling media temperature	°C
T _b	Condenser surface of vapour chamber/copper temperature	°C
T _t	Evaporation surface of vapour chamber/copper temperature	°C
T _j	Junction temperature	°C
ρ	Density	kg/m ³

REFERENCES

1. Medjahed, H., P.-E. Vidal, and B. Nogaredo, Thermo-mechanical stress of bonded wires used in high power modules with alternating and direct current modes. *Microelectronics Reliability*, 2012. **52**(6): p. 1099-1104.
2. Dupont, L., Contribution à l'étude de la durée de vie des assemblages de puissance dans des environnements haute température et avec des cycles thermiques de grande amplitude. 2006, École normale supérieure de Cachan-ENS Cachan.
3. Biela, J., et al. SiC vs. Si-evaluation of potentials for performance improvement of power electronics converter systems by SiC power semiconductors. in *Materials Science Forum*. 2010. Trans Tech Publ.
4. Kandlikar, S.G. and C.N. Hayner, Liquid Cooled Cold Plates for Industrial High-Power Electronic Devices—Thermal Design and Manufacturing Considerations. *Heat Transfer Engineering*, 2009. **30**(12): p. 918-930.
5. Wang, P., P. McCluskey, and A. Bar-Cohen, Two-Phase Liquid Cooling for Thermal Management of IGBT Power Electronic Module. *Journal of Electronic Packaging*, 2013. **135**(2): p. 021001.
6. Yin, S., K.J. Tseng, and J. Zhao, Design of AlN-based micro-channel heat sink in direct bond copper for power electronics packaging. *Applied Thermal Engineering*, 2013. **52**(1): p. 120-129.
7. Stevanovic, L., et al., Integral Micro-channel Liquid Cooling for Power Electronics. 2010. 1591-1597.
8. Brunswiler, T., et al., Interlayer cooling potential in vertically integrated packages. *Microsystem Technologies*, 2009. **15**: p. 57-74.
9. Vafai, K. and L. Zhu, Analysis of two-layered micro-channel heat sink concept in electronic cooling. *International Journal of Heat and Mass Transfer*, 1999. **42**(12): p. 2287-2297.

10. Naquiuddin, N.H., et al., Overview of micro-channel design for high heat flux application. *Renewable and Sustainable Energy Reviews*, 2018. **82**: p. 901-914.
11. Agbim, K.A., D.G. Pahinkar, and S. Graham, Integration of Jet Impingement Cooling With Direct Bonded Copper Substrates for Power Electronics Thermal Management. *IEEE Transactions on Components, Packaging and Manufacturing Technology*, 2018. **9**(2): p. 226-234.
12. Liu, Z., et al., Impingement cooling performance analysis and improvement of synthetic jets for electronic devices. *Journal of Thermophysics and Heat Transfer*, 2019. **33**(3): p. 856-864.
13. Yu, Q., et al., Cooling performance improvement of impingement hybrid synthetic jets in a confined space with the aid of a fluid diode. *Applied Thermal Engineering*, 2019. **157**: p. 113749.
14. Natarajan, G. and R. Bezama, Microjet cooler with distributed returns. *Heat transfer engineering*, 2007. **28**(8-9): p. 779-787.
15. Bhunia, A. and C. Chen, On the scalability of liquid microjet array impingement cooling for large area systems. *Journal of Heat Transfer*, 2011. **133**(6): p. 064501.
16. Gould, K., et al., Liquid jet impingement cooling of a silicon carbide power conversion module for vehicle applications. *IEEE Transactions on Power Electronics*, 2015. **30**(6): p. 2975-2984.
17. Wei, T.-W., et al. Thermal analysis of polymer 3D printed jet impingement coolers for high performance 2.5 D Si interposer packages. in 2019 18th IEEE Intersociety Conference on Thermal and Thermomechanical Phenomena in Electronic Systems (ITherm). 2019. IEEE.
18. Wei, T.-W., et al., Experimental characterization and model validation of liquid jet impingement cooling using a high spatial resolution and programmable thermal test chip. *Applied thermal engineering*, 2019. **152**: p. 308-318.
19. Wei, T., et al. First Demonstration of a Low Cost/Customizable Chip Level 3D Printed Microjet Hotspot-Targeted Cooler for High Power Applications. in 2019 IEEE 69th Electronic Components and Technology Conference (ECTC). 2019. IEEE.
20. Oliphant, K., B. Webb, and M. McQuay, An experimental comparison of liquid jet array and spray impingement cooling in the non-boiling regime. *Experimental Thermal and Fluid Science*, 1998. **18**(1): p. 1-10.
21. Fabbri, M., S. Jiang, and V.K. Dhir. Experimental investigation of single-phase micro jets impingement cooling for electronic applications. in Proceedings of the HT2003 ASME Summer Heat Transfer Conference, July. 2003.
22. Bhunia, A., Q. Cai, and C.-L. Chen. Liquid impingement and phase change for high power density electronic cooling. in Proceeding of the 41st AIAA Aerospace Sciences Meeting and Exhibit, Reno, NV, January. 2003.
23. Ditri, J., et al., Embedded Cooling of High Heat Flux Electronics Utilizing Distributed Microfluidic Impingement Jets. 2015(56901): p. V003T10A014.
24. Li, Y., et al., Thermal responses of heat pipes with different wick structures under variable centrifugal accelerations. *Applied Thermal Engineering*, 2016. **96**: p. 352-363.
25. Li, Y., et al., Thermal performance of ultra-thin flattened heat pipes with composite wick structure. *Applied Thermal Engineering*, 2016. **102**: p. 487-499.
26. Li, Y., et al., Experimental investigation of vapor chambers with different wick structures at various parameters. *Experimental Thermal and Fluid Science*, 2016. **77**: p. 132-143.
27. Li, Y., et al., Effects of vacuuming process parameters on the thermal performance of composite heat pipes. *Applied Thermal Engineering*, 2016. **99**: p. 32-41.
28. Wang, X.H., et al., Experimental investigation of the influence of surfactant on the heat transfer performance of pulsating heat pipe. *International Journal of Heat and Mass Transfer*, 2015. **83**: p. 586-590.
29. Hua, C., et al., Experimental research on the start-up characteristics and heat transfer performance of pulsating heat pipes with rectangular channels. *Applied Thermal Engineering*, 2017. **126**: p. 1058-1062.
30. Avenas, Y., et al. On the use of flat heat pipes as thermal spreaders in power electronics cooling. in Power Electronics Specialists Conference, 2002. pesc 02. 2002 IEEE 33rd Annual. 2002. IEEE.
31. Chen, Y., et al. Thermal Characterization Analysis of IGBT Power Module Integrated with a Vapour Chamber and Pin-Fin Heat Sink. in PCIM Europe 2017; International Exhibition and Conference for Power Electronics, Intelligent Motion, Renewable Energy and Energy Management. 2017.
32. Qi, F., et al. Advanced Cooling Solutions of High Power Automotive Module. in PCIM Asia 2017; International Exhibition and Conference for Power Electronics, Intelligent Motion, Renewable Energy and Energy Management. 2017.
33. Hose, C.L., et al., Integrated Vapor Chamber Heat Spreader for Power Module Applications. 2017(58097): p. V001T04A013.
34. Wang, Q., et al., Experimental investigation on EV battery cooling and heating by heat pipes. *Applied Thermal Engineering*, 2015. **88**: p. 54-60.
35. Chen, Z., et al., Design, fabrication and thermal performance of a novel ultra-thin vapour chamber for cooling electronic devices. *Energy Conversion and Management*, 2019. **187**: p. 221-231.
36. Ivanova, M., et al., Heat pipe integrated in direct bonded copper (DBC) technology for cooling of power electronics packaging. *IEEE Transactions on Power electronics*, 2006. **21**(6): p. 1541-1547.
37. Bose, J.R., N. Ahmed, and L.G. Asirvatham, Thermal performance of a vapor chamber for electronic cooling applications. *Journal of Mechanical Science and Technology*, 2017. **31**(4): p. 1995-2003.
38. Wong, S.-C., et al., A novel vapor chamber and its performance. *International Journal of Heat and Mass Transfer*, 2010. **53**(11): p. 2377-2384.
39. Xu, C., C. Gang, and M. Sakane, Prediction of stress-strain relationship with an improved Anand constitutive Model For lead-free solder Sn-3.5Ag. *IEEE Transactions on Components and Packaging Technologies*, 2005. **28**(1): p. 111-116.
40. Basaran, C., Thermomechanical stress analysis of multi-layered electronic packaging. 2003.
41. Avenas, Y., L. Dupont, and Z. Khatir, Temperature measurement of power semiconductor devices by thermo-sensitive electrical parameters—A review. *IEEE Transactions on Power Electronics*, 2012. **27**(6): p. 3081-3092.
42. Tang, Y., et al., A multi-artery vapor chamber and its performance. *Applied Thermal Engineering*, 2013. **60**(1-2): p. 15-23.
43. Infineon, Technical Information, in EconoDUAL™3 ModulmitTrench/FeldstopplIGBT4undEmitterControlled3DiodendPressFIT/NTC. 2014.



Yiyi Chen received the B.Sc and Ph.D degree in and architecture built environment engineering and sustainable energy technology from the University of Nottingham, Nottingham, UK in 2015 and 2020, respectively. In 2019, she joined Dynex semiconductor Ltd., as a senior R&D. Her current research interests include thermal management of power module, failure analysis and reliability test.

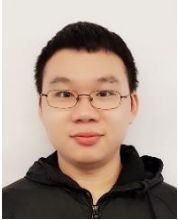


Bo Li received PhD degree in Sustainable Energy Technology from University of Nottingham in 2013. He is currently Senior Researcher Fellow of Fluids & Thermal Engineering Research Group in University of Nottingham. He is responsible for development of advanced cooling techniques for high power density semiconductor products sponsored by Advanced Propulsion project of Innovate UK. He is a member of CIBSE, and a Chartered Engineer of the UK. He has 20 years research and development experience on thermal management and fluid dynamics. His currently research interests include thermal management on advanced propulsion system including electric motors and high power density electronics.



Xuehui Wang received his bachelor degree and doctoral degree at Hefei University of Technology and Zhejiang University in 2011 and 2017, respectively. He joined the University of Nottingham as a research fellow in 2018. His main research topics are refrigeration, pulsating heat transfer and thermal management. He joined the University of Nottingham in 2018, where he worked as a research fellow focusing on the advanced cooling technologies development for

the electric motors.



Xin Wang is a currently a PhD student in Fluids & Thermal Engineering Research Group, University of Nottingham. His research focus on the thermal management of electric vehicles battery system. Now he is studying the pulsating heat pipe operating with novel working fluid and deposition pattern.



Yuying Yan obtained his PhD in Mechanical Engineering at City University of London. He is Professor of Thermofluids Engineering, Li Dak Sum Chair Professor in Thermofluids Engineering at University of Nottingham. With more than 30 years experience in fluid flow and heat transfer, he is a member of EPSRC Peer Review College; Associate Editor of Elsevier Journal - Case Studies of Thermal Engineering, Editorial Board member

for International Journal of Heat and Mass Transfer, Nature Publishing Group's multidisciplinary Journal: Scientific Reports, Journal of Bionic Engineering, Automotive Innovation, and Elsevier Journal of Thermal Science and Engineering Progress. He is fellow of International Society of Bionic Engineering. He has supervised more than 30 PhD students and authored or co-authored more than 200 academic papers in refereed journals.



Xiang Li received the B.S. degree in vacuum electronics technology from the University of Electronic Science and Technology of China, Chengdu, China, in 2009, and the Ph.D. degree in electronic engineering from the School of Electronic Engineering and Computer Science, Queen Mary University of London, London, U.K. in 2016. In 2016, he joined Lancaster University, Lancaster, U.K., as a research associate in vacuum electronic devices. In 2017, he joined Dynex

Semiconductor Ltd., as a senior R&D engineer in power semiconductor modules.

His current research interests include power semiconductor device modeling, analysis as well as test, power module thermal management, and power converter electromagnetic interference.

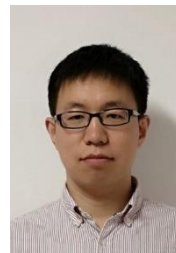


Yangang Wang received PhD degree in Microelectronics and Solid-State Electronics from Peking University in 2007. He joined the R&D Centre of CRRC Dynex Semiconductor Ltd in the UK as a Principal Engineer in 2012, and is currently the Vice Director of the R&D Centre, Dynex Semiconductor, CRRC Times Electric co., Ltd. He is leading the department responsible for development of advanced Si and WBG power semiconductor products. He is a senior member of IEEE, member of IET and a Chartered Engineer of the UK. He has more than 20 year research and development work experience on Microelectronics and Power Electronics. His currently research and development activities include design/simulation, packaging, test/characterization, failure analysis, reliability and lifetime prediction etc for power Si and WBG semiconductor devices.



Fang Qi received the B.S. degree in electrical engineering from the Beijing jiaotong University of China, Beijing in 2007. In 2007, he joined CRRC as a power electronics technology application engineer. In 2014, he joined Dynex semiconductor Ltd. as a senior R&D engineer in power module semiconductor modules. Now, he joined Coresing semiconductor technology CO., LTD, he is leading the R&D center for advanced power semiconductor.

His currently research and development activities include design, simulation, packaging, testing, failure analysis, reliability and lifetime prediction etc for advanced power semiconductor.



Helong Li received B.Sc. (2010) and M.Sc. (2012) degrees from Harbin Institute of Technology, China, both in electrical engineering. In 2015, he got his PhD degree from Department of Energy Technology, Aalborg University. From 2016 to 2019, he was working in Dynex Semiconductor Ltd, UK, focusing on power semiconductor packaging. Since 2019, he has been working for Cree Europe GmbH, focusing on SiC devices in automotive applications (power module, traction inverter, OBC, etc). His interests and research works involves power semiconductor (IGBT and SiC MOSFETs) packaging and applications.